Composites: Part B 60 (2014) 515–522

Contents lists available at ScienceDirect

Composites: Part B

journal homepage: www.elsevier.com/locate/compositesb

Characterization and catalytic properties of some perovskites

Nicolae Rezlescu [a,*], Elena Rezlescu [a], Paul Dorin Popa [a], Corneliu Doroftei [b], Maria Ignat [c]

[a] National Institute of Research and Development for Technical Physics, Iasi, Romania
[b] "Al. I. Cuza" University, Faculty of Physics, Iasi, Romania
[c] "Al. I. Cuza" University, Faculty of Chemistry, Iasi, Romania

ARTICLE INFO

Article history:
Received 22 August 2013
Received in revised form 18 November 2013
Accepted 3 January 2014
Available online 9 January 2014

Keywords:
B. Microstructures
D. Electron microscopy
D. Surface analysis
E. Heat treatment

ABSTRACT

The perovskite oxides are promising catalysts for VOCs combustion. The purpose of this work is to comparatively evaluate catalytic activity of some simple perovskites with various cationic compositions in combustion reactions of acetone, benzene, propane and Pb free gasoline. Nanometer particles of nominal composition: $GdAlO_3$, $SrMnO_3$, $SrCoO_3$ and $MnFeO_3$ were prepared by the sol–gel self-combustion method followed by heat treatment at 1000 °C in air. The samples were characterized by X-ray diffraction, scanning electron microscopy, energy dispersive X-ray spectroscopy and nitrogen adsorption/desorption isotherms. All samples have perovskite type structure and the crystallite size is in the range of 40–89 nm. Catalytic testing evidenced that the degree of the catalytic activity varied considerably with the perovskite composition. Among the four perovskites, $SrMnO_3$ is generally the most active catalyst at low temperatures. $MnFeO_3$ and $SrCoO_{3-x}$ catalysts proved high catalytic activity in acetone conversion only. The change in the catalytic activity as a result of the modification of the perovskite composition may be explained either by the different reactivity of the active oxygen species involved in the catalytic oxidation, or by the variation in the number of active sites on the perovskite surface determined by the specific structural properties of each perovskite.

© 2014 Elsevier Ltd. All rights reserved.

1. Introduction

The perovskite oxides are proved to be highly active catalysts for oxidation reactions in connection with air pollution control [1]. They are considered as potential substitutes for noble metal catalysts, which are expensive [2]. Perovskite catalysts combine low cost, thermo-chemical stability at high operating temperature and satisfactory catalytic activity [3–14].

Although the perovskites are potentially suitable for oxidation of the volatile organic compounds (VOCs), most of research on the catalytic activity of the perovskites has focused on methane combustion [15–17]. The catalytic combustion of methane has received attention mainly due to the possibility of lowering the combustion temperature, thus practically reducing emissions of NO_x, CO and unburned hydrocarbons. We extended this research and explored the role of perovskites in the catalytic combustion of other volatile organic compounds.

The perovskite structure is generally described by the formula AMO_3, where A is usually an alkaline earth or rare earth and M is a transition metal cation (most frequently manganese or cobalt). The A cation is larger than the M cation. The catalytic activity of perovskite-type oxides in VOCs oxidation is essentially controlled by the M-site cation and can be improved by substitution of another A-site or M-site cation [17–19].

Many researches have suggested that oxygen vacancies in the perovskite oxides play a major role in catalytic oxidations, although the origin of their catalytic activity is still debated [11,20,21]. By partial or total replacement of the A^{3+} or M^{3+} ions with elements of different valence in the AMO_3 perovskite one can generate oxygen vacancies, which are preferential points for O_2 adsorption [19]. Important for perovskite activity as catalyst in the catalytic flameless combustion of VOCs is the oxygen mobility [22–24]. The oxygen mobility inside the perovskite lattice is affected by the nature of the A-site cation [25] and increases proportionally with the concentration of oxygen vacancies.

For any practical wide-scaled applications, the price of catalyst has to be reasonably low. To meet this constraint simple and inexpensive methods for perovskite synthesis are necessary. The preparation of perovskite type oxide compound involves a solid-state reaction of its precursor oxides to form the AMO_3 structure. This requires an exposure of the precursor oxides to high temperature leading to a low specific surface area of the catalyst. Even though the best catalytic performances in catalytic combustion are exhibited by La- or Sr-based perovskites containing Co, Fe or Mn as M cation [16], the greatest limitation for their applications is their low surface area that appears to be a serious disadvantage. To overcome this drawback, a number of alternative preparation

* Corresponding author. Tel.: +40 0232216895; fax: +40 0232231132.
E-mail address: nicolae.rezlescu@gmail.com (N. Rezlescu).

1359-8368/$ - see front matter © 2014 Elsevier Ltd. All rights reserved.
http://dx.doi.org/10.1016/j.compositesb.2014.01.006

methods have been tried in an attempt to lower sintering temperature for perovskite synthesis. In the present work a non-conventional method combining sol–gel route with self-combustion [26–28] was used to prepare four simple perovskites: $SrMnO_3$, $SrCoO_3$, $MnFeO_3$ and $GdAlO_3$. Following this method, the synthesis conditions can be controlled by subsequent heat treatments and grain sizes substantially smaller than those obtained by the conventional ceramic method can be achieved. We analyzed comparatively the catalyst properties of these perovskites in the total oxidation of some dilute gases: acetone, benzene, propane and Pb free gasoline. Influence of various catalyst parameters (chemical composition, crystallite size and specific surface area) and process parameters (reaction temperature, conversion degree, reaction rate and activation energy) on VOCs catalytic combustion has been investigated.

2. Experimental

2.1. Preparation of perovskites

The performance of a catalyst depends on its physical–chemical properties which are strongly affected by the synthesis technique of the catalyst. In the present work the sol–gel-self-combustion method described in our previous papers [28–31] was used to prepare $SrMnO_3$ (SMP), $SrCoO_3$ (SCP), $MnFeO_3$ (MFP) and $GdAlO_3$ (GAP) nanocrystalline perovskite powders. This method included the following steps: (1) dissolution of metal nitrates in deionized water; (2) polyvinyl alcohol (10% concentration) addition to nitrate solution to make a colloidal solution; (3) NH_4OH (10% concentration) addition to increase pH to about 8; (4) stirring at 80 °C to turn the sol of metal hydroxides into gel; (5) drying the gel at 100 °C; (6) self-combustion of the dried gel; (7) calcinations at 500 °C for 30 min of the burnt powder to eliminate any residual ceramic compounds; (8) heat treatment of the powders. The heat treatment was performed at 1000 °C for 7 h. The migration of ions for the formation of the perovskite structure demands a long treatment time.

2.2. Physical–chemical characterization of the perovskites

The specific surface area (S_{BET}) of the samples was determined from the nitrogen sorption isotherms at the temperature of liquid nitrogen using the standard Brunauer, Emmet and Teller method [32]. Adsorption/desorption isotherms were obtained using Nova-2200 apparatus, after out gassing of samples at 300 °C overnight. The pore size distribution (PSD) curves were obtained using BJH (Barret–Joygner–Halenda) method [32].

Information about the crystallographic phases and crystallite sizes was obtained by X-ray diffraction (XRD). The average crystallite sizes were estimated using the Scherrer equation:

$$D_{XRD} = \frac{0.9\lambda}{\beta \cos\theta}, \quad (1)$$

where λ is radiation wavelength, β is the half width of the peak and θ is the Bragg diffraction peak angle which can be applied for crystallites up to 100–150 nm in diameter. A PANALYTICAL X' PERT PRO MPD powder diffractometer was used for XRD measurements on powder samples. Cu Kα radiation (λ = 1,542512 Å), a scanning rate of 2 °/min and a spectral resolution of 0.008° were used. Patterns were collected in the range $20° \leqslant 2\theta \leqslant 80°$.

The visualization of the morphology (SEM images) was performed with the scanning electron microscope (JEOL-200 CX). The chemical composition of the surface particles was examined with Energy Dispersive X-ray Spectrometer (EDS). Incident electron beam energies from 0 to 16 keV have been used.

2.3. Catalytic testing

Catalytic flameless combustion reactions of acetone, benzene, propane and Pb free gasoline in the presence of the perovskite catalyst were performed in a flow quartz tubular reactor (flow rate of 100 cm^3/min and VOC concentration in air of 1–2‰) with an inner diameter of 7 mm. The powder catalyst (typically 0.3–0.5 g) was sandwiched between two glass wool layers in the isotherm zone of the reactor, which is heated by a tubular electric furnace. Catalytic tests were performed at gas hourly slacer velocity (GHSV) of 5100 h^{-1} in the temperature range 20–550 °C. The increase of the temperature was made in steps of 50 °C. At every predetermined temperature the gas concentration at the exit of reactor was measured by a photo-ionization detector (PID-TECH) for VOCs. Details on the set-up for catalytic tests at atmospheric pressure are given in a previous paper [30]. The catalytic activity of the perovskites under study was evaluated in terms of the gas conversion η calculated as:

$$\eta = \frac{c_{in} - c_{out}}{c_{in}} \times 100\%, \quad (2)$$

where c_{in} and c_{out} are the inlet and outlet gas concentration, respectively. Data were collected when the flameless catalytic combustion had reached a steady state, after about 20 min at each temperature. These experiments were repeated with decreasing temperature and similar results were obtained. The catalysts were not deactivated during testing.

3. Results and discussion

3.1. Structural characteristics of perovskites

The room temperature XRD patterns for samples presented in Fig. 1 were indexed as perovskite type structure. Identification was performed by comparing the patterns to a known standard. $GdAlO_3$ was identified as orthorhombic perovskite phase (Fig. 1a), $SrMnO_3$ and $SrCoO_3$ were indexed as hexagonal perovskite type structure (Fig. 1b and c) and $MnFeO_3$ perovskite crystallizes in the

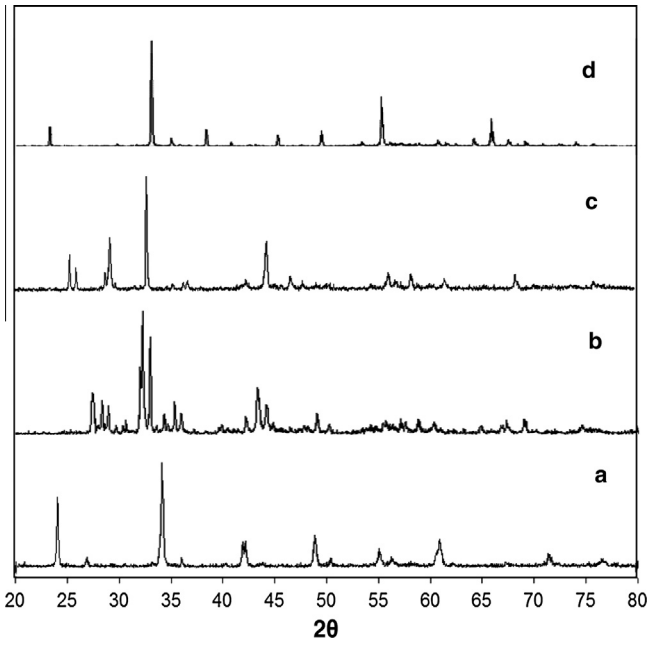

Fig. 1. XRD patterns of the studied perovskites: (a) $GdAlO_3$, orthorombic perovskite (PDF 24-419); (b) $SrMnO_3$, hexagonal perovskite (PDF 72-197); (c) $SrCoO_{3-x}$, hexagonal perovskite (PDF 40-1018); (d) $MnFeO_3$, cubic perovskite (PDF 75-894).

Table 1
Phase composition, lattice parameter, average crystallite size and X-ray density of the investigated samples.

Sample	Phases by XRD analysis	Lattice parameter (Å)	D_{XRD}[a] (nm)	d_X (g/cm^3)
$SrMnO_3$	Hexagonal perovskite (space group P63/mmc)	a = 5.459 c = 9.090	88.9	5.45
$SrCoO_3$	Hexagonal perovskite (space group)	a = 5.485 c = 4.137	59.9	6.45
$MnFeO_3$	Cubic perovskite (space group Ia3)	a = 9.400	59.2	5.08
$GdAlO_3$[b]	Orthorhombic perovskite (space group Pbnm)	a = 5.250 b = 5.302 c = 7.440	39.6	7.43

[a] Crystallite size calculated with Scherrer's equation.
[b] Data for $GdAlO_3$ catalyst are taken from [28].

cubic system (Fig. 1d). Both the hexagonal and the orthorhombic perovskite type structures are derived from the distorted cubic perovskite structure.

The phase composition, lattice parameter, average crystallite size and X-ray density of the investigated samples after heat treatment at 1000 °C are summarized in Table 1. In this study strontium cobaltite was identified as $SrCoO_{3-x}$ by reference to the diffraction pattern standard (Pdf nr. 40-1018). This composition with oxygen deficit indicates that the valence of cobalt is 3+. The Sr bivalent cations (Sr^{2+}) cause higher oxidation states of cobalt, but because Co^{4+} is instable, an oxygen release takes place, so that oxygen vacancies are formed.

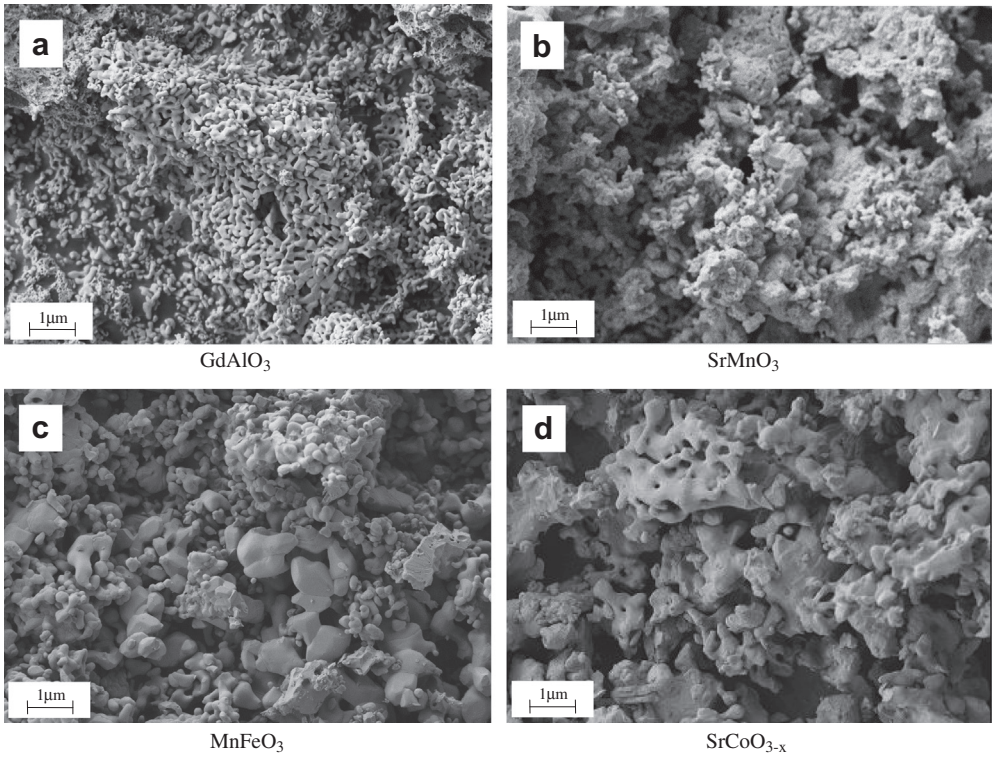

Fig. 2. SEM images of: (a) $GdAlO_3$, (b) $SrMnO_3$, (c) $MnFeO_3$ and (d) $SrCoO_{3-x}$ perovskites.

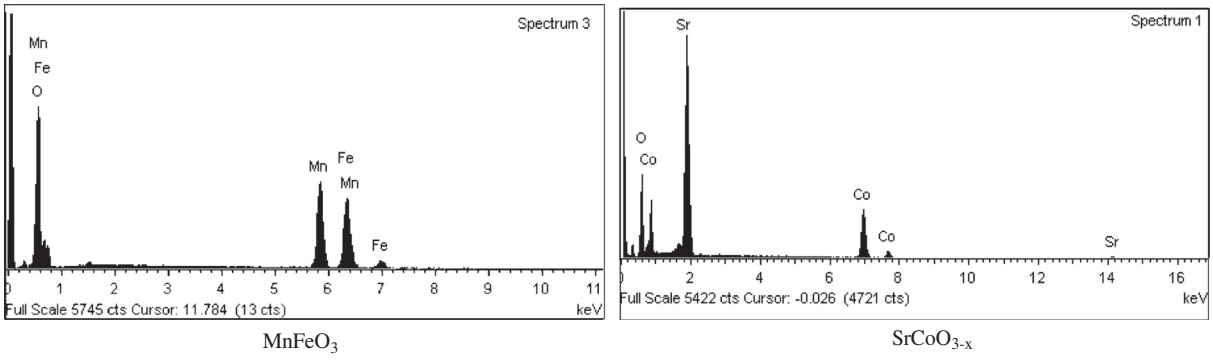

Fig. 3. EDS spectra for two perovskites: $MnFeO_3$ and $SrCoO_{3-x}$.

Table 2
EDS analysis of perovskite powders after heat treatment at 1000 °C.

Perovskite AMO_3	*O* (at.%)	*A* (at.%)	*M* (at.%)	$\frac{A}{A+M}$	$\frac{M}{A+M}$
$SrMnO_3$	62.11	21.50	16.39	0.56	0.44
$SrCoO_3$	60.80	20.84	18.36	0.53	0.47
$MnFeO_3$	62.75	19.91	17.34	0.54	0.46
$GdAlO_3$[a]	64.18	17.82	18.00	0.497	0.503

[a] Data for $GdAlO_3$ are taken from [28].

The size of crystallites calculated from X-ray diffraction data (D_{XRD}) was found to be in the range 40–89 nm and this indicated that the perovskites prepared by sol–gel self-combustion route have nano-sized crystallites. The higher X-ray density of $GdAlO_3$ perovskite was expected since the Gd atom is heavier than the other atoms.

3.2. Micromorphology and textural characteristics

The morphologies of the samples examined by SEM are shown in Fig. 2. $GdAlO_3$ is characterized by uniform distribution of small particles (about 100 nm) (Fig. 2a). A striking change in the morphology of the other three perovskites was observed (Fig. 2b, c and d). In these samples the particles did not show a distinct shape and the particle size appreciated by linear intercept method is larger, up to 200 nm, regardless of the chemical composition. Also, the clustering of the particles into mini- or macro-aggregates with irregular shapes and sizes is evident.

Fig. 3 presents the EDS spectra for two perovskites only ($SrCoO_3$ and $MnFeO_3$) and the elemental composition in all the monophase perovskites is given in Table 2. One can remark the purity of the chemical composition; any foreign element is absent. Moreover the composition of the samples is similar to the nominal one, AMO_3, i.e. the A/(A + M) or M/(A + M) ratio is close to 0.5.

The nitrogen adsorption/desorption isotherms at 77 K are shown in Fig. 4. The isotherms can be classified as type IV with a small H3 type hysteresis loop, according to IUPAC classification [32]. The inflexion point of isotherms indicates the stage at which monolayer coverage is complete and multilayer adsorptions begin to occur. The pore size distribution (PSD) obtained from nitrogen desorption isotherms is shown inset of Fig. 4. The pore sizes (9–20 nm) fall within mesoporous region (2–50 nm) [32]. The specific surface areas (S_{BET}) and total pore volume are given in Table 3. It can be noted that the perovskite composition has an impact on the surface area. The increase in S_{BET} area is in this order: SCP < SMP < MFP < GAP. The largest BET surface area (10 m^2/g) has $GdAlO_3$ perovskite, which exhibits the smallest crystallite size (40 nm). The total replacement of Gd^{3+} results in a decrease in the BET surface area as a consequence of the presence of agglomerations. The lowest values of S_{BET} (of about 2 m^2/g) have been found in $SrCoO_{3-x}$ and $SrMnO_3$ perovskites, which have higher values for the particle size and smaller pore volume. S_{BET} values measured (2–10 m^2/g) are comparable to those reported by other authors [33] for perovskites with similar chemical composition.

Using S_{BET} data, the average particle size D_{BET} was calculated with the formula [32]:

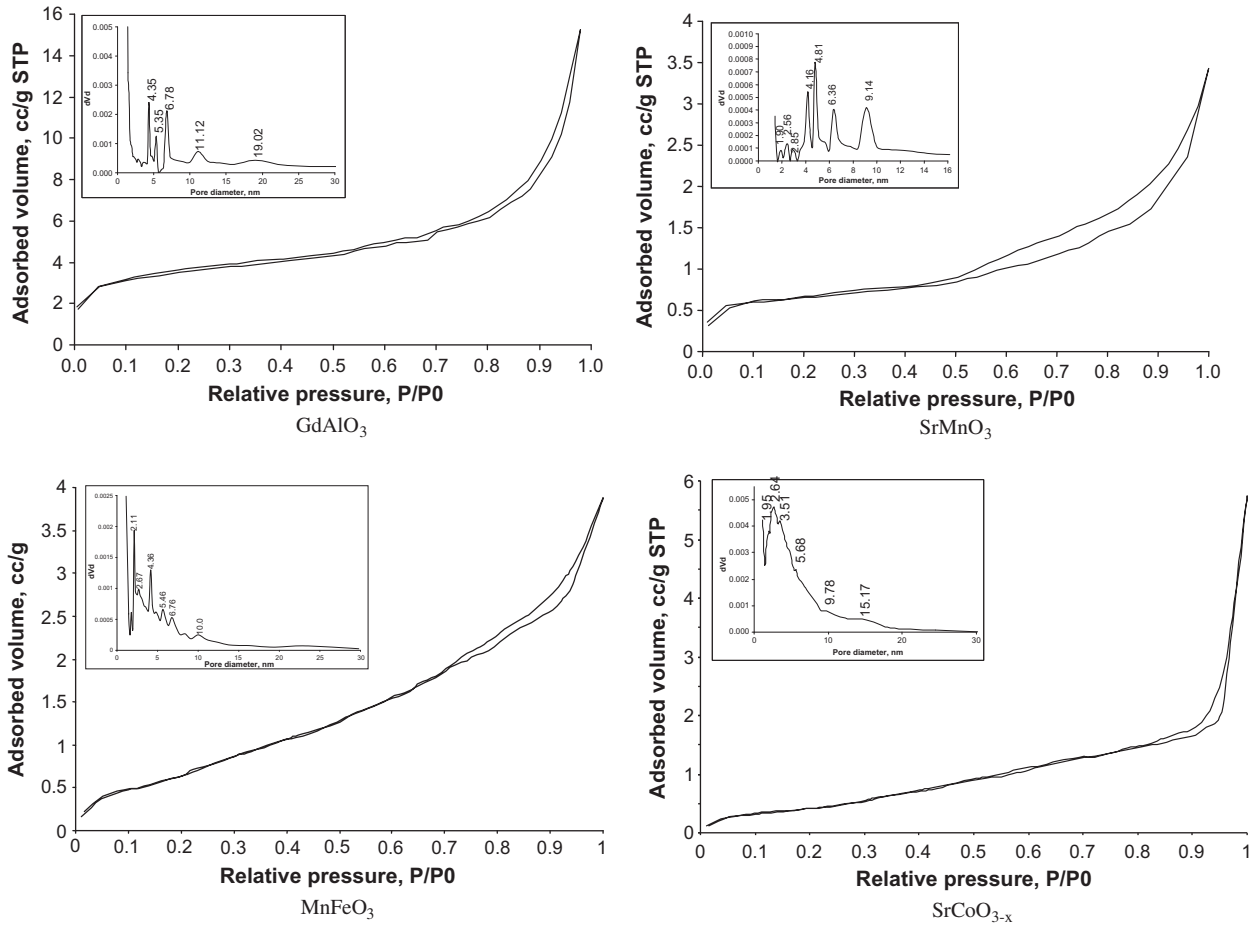

Fig. 4. N_2 adsorption/desorption isotherms (inset shows calculated BJH plots).

Table 3
Surface characteristics for the perovskites after 1000 °C heat treatment.

Perovskite composition	S_{BET} (m^2/g)	D_{BET}[a] (nm)	Total pore volume (cm^3/g)
$SrMnO_3$	2.2	500	9.75×10^{-4}
$SrCoO_3$	1.9	490	3.05×10^{-3}
$MnFeO_3$	3.2	370	4.45×10^{-3}
$GdAlO_3$[b]	9.8	81	1.80×10^{-2}

[a] Particle size calculated from S_{BET} [29].
[b] Data for $GdAlO_3$ are taken from [28].

$$D_{BET} = \frac{6}{S_{BET} \cdot d_X}, \quad (3)$$

where 6 is the shape factor and d_X is the X-ray density. One can see in Table 3 that D_{BET} is substantially greater than the X-ray crystallite size D_{XRD} (Table 1).

3.3. Catalytic activity of perovskites

The catalytic performances of the four simple perovskites in the flameless combustion of some VOCs were investigated in the temperature range 20–550 °C. The results are presented in Fig. 5, where the gas conversion was plotted as a function of the reaction temperature for each perovskite composition. One can note the followings:

(i) The catalytic activity of the perovskite catalyst is influenced by the reaction temperature. Increasing the reaction temperature facilitates gas combustion.

(ii) The catalytic activities of the perovskites of different compositions differ substantially, consistent with the results reported by Seyfi et al. [19]. Fig. 5 shows an improved catalytic activity of strontium manganite catalyst compared to that of gadolinium aluminate catalyst. Their different specific surface areas cannot explain the difference in the activity of the two samples. The specific surface area of $GdAlO_3$ is 10 m^2/g while for $SrMnO_3$ is smaller, of 2.2 m^2/g (Table 3).

(iii) The gas combustion over $SrMnO_3$ catalyst started at much lower temperatures (at about 100 °C) compared to the other perovskites. The greater activity of $SrMnO_3$ catalyst toward the conversion of VOCs indicates availability of reactive oxygen species on the catalyst surface. This suggests oxygen may be less anchored on the perovskite surface and be more available for VOCs oxidation, probable because of the presence of a noteworthy amount of Mn^{4+} ions.

(iv) An interesting result was obtained for manganese ferrate ($MnFeO_3$) (Fig. 5c) and for strontium cobaltite ($SrCoO_{3-x}$) (Fig. 5d). Regardless of the chemical composition, the two catalysts exhibited high catalytic activity only towards acetone conversion and proved poor catalytic performance in catalytic combustion of propane, benzene and gasoline. The reasons for such a selective catalytic activity are not yet clear. This behavior may be related to some rearrangement of their lattice structure and, as a consequence, of the active site structure, on which the catalytic properties of these perovskites depend. It is interesting to point out the strong influence of temperature on the acetone conversion over the $MnFeO_3$ catalyst. The acetone conversion started at a low temperature (150 °C) and the conversion

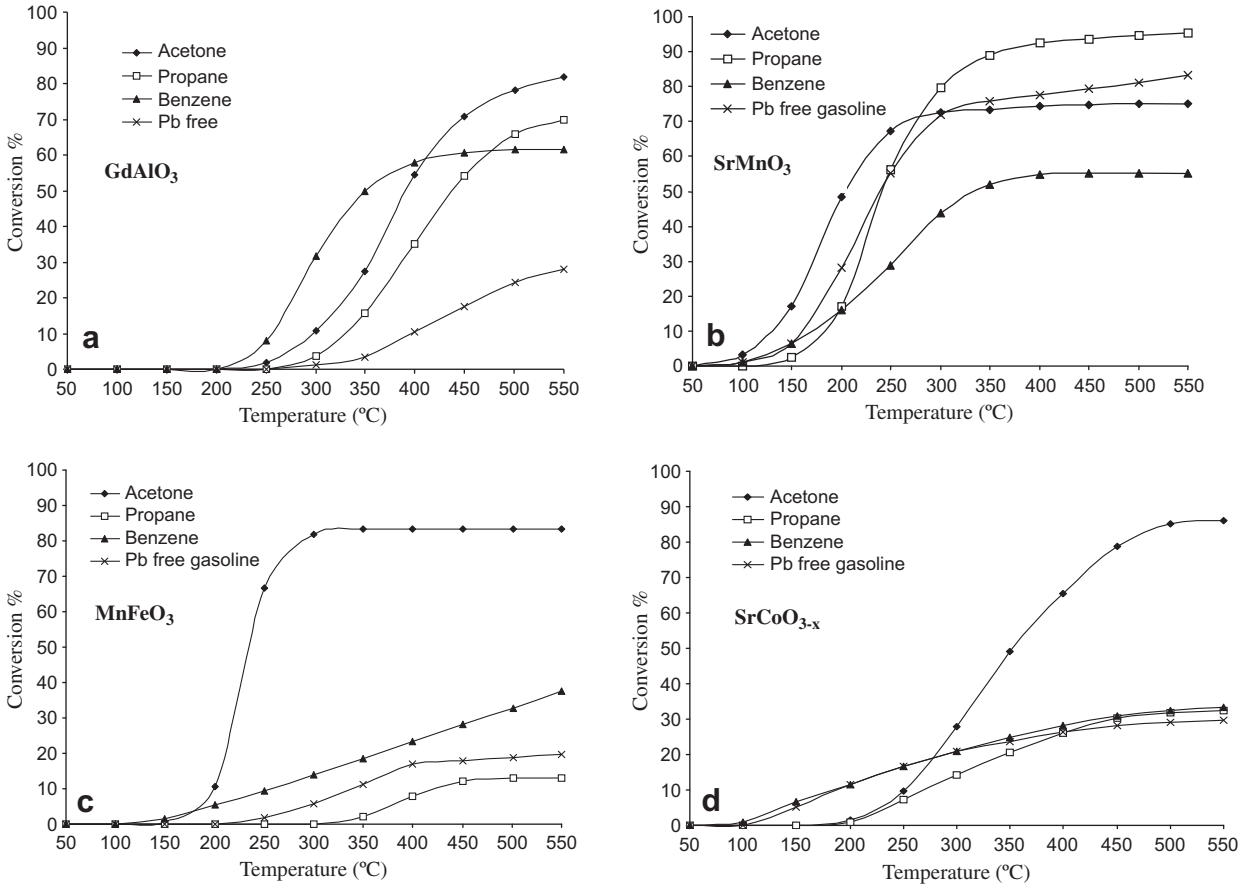

Fig. 5. Conversion vs. temperature for catalytic flameless combustion of acetone, propane, benzene and Pb free gasoline over (a) $GdAlO_3$, (b) $SrMnO_3$, (c) $MnFeO_3$ and (d) $SrCoO_{3-x}$ perovskites.

Table 4
T_{10}, T_{50} and kinetic parameters (reaction rate[a] and activation energy[b]) for perovskite catalysts.

VOCs	$GdAlO_3$				$SrMnO_3$				$MnFeO_3$				$SrCoO_3$			
	T_{10} (°C)	T_{50} (°C)	Reaction rate (μmol s^{-1} m^{-2})	Activation energy (kJ/mol)	T_{10} (°C)	T_{50} (°C)	Reaction rate (μmol s^{-1} m^{-2})	Activation energy (kJ/mol)	T_{10} (°C)	T_{50} (°C)	Reaction rate (μmol s^{-1} m^{-2})	Activation energy (kJ/mol)	T_{10} (°C)	T_{50} (°C)	Reaction rate (μmol s^{-1} m^{-2})	Activation energy (kJ/mol)
Acetone	295	390	6.7×10^{-2}	89	130	200	140×10^{-2}	37	200	230	65×10^{-2}	98	250	325	16×10^{-2}	41
Propane	330	440	7.8×10^{-2}	71	180	240	9.8×10^{-2}	31	400	–	6.1×10^{-2}	80	270	–	3.8×10^{-2}	48
Benzene	260	350	6.5×10^{-2}	68	175	325	26×10^{-2}	35	255	–	17×10^{-2}	45	190	–	56×10^{-2}	44
Pb free gasoline	390	–	4.2×10^{-1}	62	160	240	55×10^{-2}	36	340	–	12×10^{-2}	47	190	–	11×10^{-2}	40

T_{10} and $T_{50\%}$ – temperatures required for 10% and 50% gas conversion.
[a] Reaction rate for VOC concentration at low conversion per unit surface area of catalyst.
[b] Apparent activation energy for low conversions.

degree sharply increased from 10% to 80% as the temperature increased from 200 to 300 °C (Fig. 5c). This behavior was not observed with the other perovskites. In contrast with the $MnFeO_3$ catalyst, the $SrCoO_{3-x}$ catalyst started the acetone conversion near 200 °C and 80% acetone conversion was obtained at a higher temperature, of 450 °C. A better conversion of the four gases was obtained over the $GdAlO_3$ and $SrMnO_3$ catalysts.

The activity data collected during the flameless combustion of VOCs over the four perovskite catalysts are presented in Table 4. T_{10} and T_{50} are the temperatures required for 10% and 50% conversion of a gas and can be obtained from the conversion versus temperature curve. Temperature T_{50} is usually chosen as the main indicator of catalytic activity of a given catalyst. At T_{50} temperature the catalytic activity for the total oxidation of gases is sufficiently high and the interactions between catalyst surface and reactants are intense. The lower this parameter is, the higher the activity of the catalyst is. $SrMnO_3$ seems to be a more active catalyst than the others. Its temperatures T_{10} and T_{50} are much lower than those for the other catalysts (Table 4).

Table 4 also includes the values of the kinetic parameters (apparent activation energy and reaction rate) for gas oxidation over the four perovskite catalysts. The apparent activation energies for the catalytic reactions were calculated by means of the Arrhenius type plot of the natural logarithm of the rate constant k at low conversion (bellow 10–15%) versus inverse temperature ($1/T$). This plot is a straight line and from its slope the apparent activation energy was calculated. One can observe that the reaction rate normalized to specific area changes from 3.8×10^{-2} μmol s^{-1} m^{-2} to 140×10^{-2} μmol s^{-1} m^{-2}. The higher the reaction rate is higher, the more active is the catalyst. Note also the wide variation in activation energies from 40 kJ/mol ($SrCoO_3$ toward gasoline combustion) to 98 kJ/mol ($MnFeO_3$ toward acetone combustion). The smallest values (31–37 kJ/mol) of the apparent activation energy were obtained for the $SrMnO_3$ catalyst with the best catalytic activity. The differences observed between the activation energies suggest that the nature of the catalytic sites differs from one perovskite to the others. The smaller values of the activation energy for the samples $SrCoO_3$ and $SrMnO_3$ can indicate a contribution of the mass transfer effects [34]. The values of the kinetic parameters obtained by us are comparable to those presented by other authors for other perovskite type oxides and VOCs [35,36].

The results presented in Fig. 6 clearly indicate that the chemical composition of the perovskite catalysts and gas nature have a significant influence on the catalytic performance in VOCs combustion. Also, it is evident that $SrCoO_3$ and $MnFeO_3$ catalysts favor the oxidation of acetone only. These catalysts were able to convert 85% acetone at 500 °C whereas the conversion of the other gases was below 30%. The comparison shown in Fig. 6 indicates that, among the four studied perovskite samples, the most preferred catalyst, which shows the highest catalytic activity at low temperatures, is $SrMnO_3$ despite its small surface area (2.2 m^2/g). This catalyst was able to convert 95% propane, 83% Pb free gasoline and 75% acetone at 500 °C. The low specific area of the $SrMnO_3$ perovskite does not seem to take part in the higher activity of this catalyst. The improved catalytic activity of $SrMnO_3$ may be ascribed to the higher oxygen mobility due to the oxygen vacancies generated by the presence of manganese ion with variable valence. The difference in the catalytic activity of the four perovskites cannot be explained by their different specific surfaces. A dependence of activity on surface area was not found. Other factors, such as structural defects and oxygen mobility, probably control the catalytic activity of these perovskite catalysts.

There are many hypotheses about the mechanism of oxidation of VOCs on the oxide compounds. According to one accepted

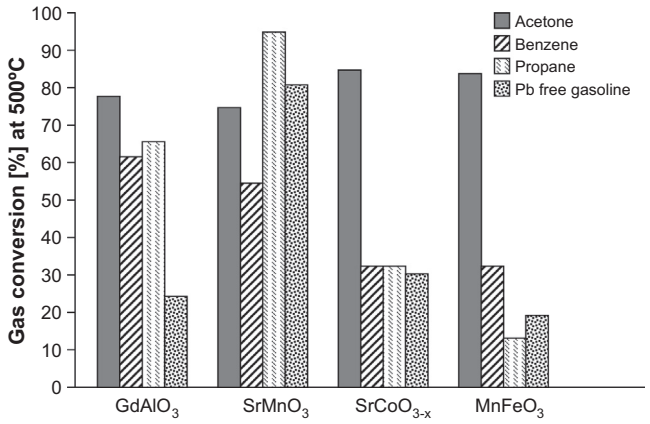

Fig. 6. Influence of the chemical composition of perovskite catalysts on the gas conversion at 5000C.

opinion, at low temperatures (below 400 °C) the catalytic activity of the perovskite oxides in the total oxidation reactions of the gases is largely determined by the amount of weakly bound surface oxygen species [37] which in turn depends on the presence of oxygen vacancies. The weaker the oxygen binding at the catalyst surface is, the more active the catalyst for complete oxidation of gases is [38–40]. The surface oxygen species (O^-, O_2^-, O^{2-}) involved in the catalytic combustion may come from the gaseous molecular oxygen and from the lattice oxygen [41,42]. The interaction of surface active oxygen species with reactants has an important role in mechanism of VOCs total oxidation (suprafacial mechanism) over perovskites oxide and this is widely accepted to explain the gas oxidation over mixed oxide catalysts [37].

In the present study, the difference in the catalytic activity of the four perovskite catalysts in the combustion of acetone, propane, benzene and Pb free gasoline may be explained by either the different reactivity or amount of the active oxygen species involved in the combustion reaction, or by variation in the number of active sites on the perovskite surface determined by the specific structural properties of each perovskite. The gas oxidation activity over perovskite catalysts is related to the ability of surface oxygen to activate gas leading to the removal of surface oxygen and to the ability of gas phase oxygen or bulk oxygen to fill surface oxygen vacancies.

The involvement of the lattice oxygen cannot be avoided in catalytic gas oxidation. According to Arai et al. [16] gas oxidation over perovskite oxides can be explained by assuming the involvement of both adsorbed oxygen and lattice oxygen. The degree in which the lattice oxygen is involved in the catalytic process depends on the oxygen mobility in the volume of the crystal lattice, the gas oxidation rate being determined by the rate of oxygen diffusion in the oxygen sublattice. Lattice defects facilitate the oxygen diffusion (via vacancy mechanism [37]) from the volume to the catalyst surface. Hence, structural defects and oxygen mobility are important factors controlling the catalytic activity of perovskites. In this study, the compositional changes may affect the concentration of oxygen defects, the structure and activity of the surface active sites. Such factors may account for the change in the catalytic properties as a result of the modification of the perovskite composition.

4. Conclusions

By sol–gel self-combustion method followed by heat treatment at 1000 °C, several nanostructured perovskites with various compositions ($SrMnO_3$, $SrCoO_3$, $MnFeO_3$ and $GdAlO_3$) were prepared for catalyst applications. The X-ray diffraction confirmed the perovskite phase and nanosize of the perovskite crystallites (40–89 nm). The catalytic tests of the perovskites in the flameless catalytic combustion of acetone, benzene, propane and Pb free gasoline evidenced that the degree of the catalytic activity varied considerably with the composition of perovskite. The catalyst containing strontium and manganese ($SrMnO_3$) is generally more active than the other catalysts. $MnFeO_3$ and $SrCoO_{3-x}$ perovskites proved high catalytic activity in acetone conversion only and poor catalytic performance toward propane, benzene and gasoline combustion. It is worth noting the sharp increase of the acetone conversion over $MnFeO_3$, from 10% to 80% as the temperature increases from 200 to 300 °C. The change in the catalytic properties as result of modification of perovskite composition could not be correlated with their specific surface area (2–10 m^2/g).

A possible explanation for the change in the catalytic properties as result of modification of perovskite composition may be either the different reactivity of the active oxygen species involved in the catalytic oxidation, or the variation in the number of active sites on the perovskite surface determined by the specific structural properties of each perovskite.

Acknowledgement

This work was supported by a grant of the Romanian National Authority for Scientific Research, CNST – UEFISCDI, project number PN-II-ID-PCE-2011-3-0453.

References

[1] Didenko OZ, Kosmambetova GR, Strizhak PE. Synthesis of nanosized ZnO/MgO solid and its catalytic activity for CO oxidation. Chinese J Catal 2008;29:1079–83.
[2] Hosseini SA, Niaei A, Salari D, Aghzadeh F. Nanostructure copper-exchanged ZSM-5 catalytic activity for conversion of volatile organic compounds (toluene and ethyl acetate). Chinese J Chem 2010;28:143–8.
[3] Rosso I, Saracco G, Specchia V, Garrone E. Sulphur poisoning of $LaCr_{0.5-x}Mn_xMg_{0.5}O_3$ center dot yMgO catalysts for methane combustion. Appl Catal, B 2003;40:195–205.
[4] Sadjadi MS, Mozaffari M, Enhessari M, Zare K. Effects of $NiTiO_3$ nanoparticles supported by mesoporous MCM-41 on photoreduction of methylene blue under UV and visible light irradiation. Superlattices Microstruct 2010;47:685–91.
[5] Campagnoli E, Tavares A, Fabbrini L, Rossetti I, Dubitsky YA, Zaopo A, et al. Effect of preparation method on activity and stability of $LaMnO_3$ and $LaCoO_3$ catalysts for the flameless combustion of methane. Appl Catal, B 2005; 55:133–9.
[6] Rossetti I, Forni L. Catalytic flameless combustion of methane over perovskites prepared by flame-hydrolysis. Appl Catal, B 2001;33:345–52.
[7] Fabbrini L, Rossetti I, Forni L. Effect of honeycomb supporting on activity of $LaBO_3$ delta perovskite-like catalysts for methane flameless combustion. Appl Catal, B 2006;63:131–6.
[8] Leanza R, Rossetti I, Fabbrini L, Oliva C, Forni L. Perovskite catalysts for the catalytic flameless combustion of methane – preparation by flame-hydrolysis and characterisation by TPD-TPR-MS and EPR. Appl Catal, B 2000;28:55–64.
[9] Alifanti M, Kirchnerova J, Delmon B. Effect of substitution by cerium on the activity of $LaMnO_3$ perovskite in methane combustion. Appl Catal, A 2003;245:231–43.
[10] Forni L, Rossetti I. Catalytic combustion of hydrocarbons over perovskites. Appl Catal, B 2002;38:29–37.
[11] Spinicci R, Tofanari A, Delmastrto A, Mazza D, Ronchetti S. Catalytic properties of stoichiometric and non-stoichiometric $LaFeO_3$ perovskite for total oxidation of methane. Mater Chem Phys 2002;76:20–5.
[12] Cimino S, Benedetto Di, Pirone R, Russo G. Transient behaviour of perovskite-based monolithic reactors in the catalytic combustion of methane. Catal Today 2001;69:95–103.
[13] Ponce S, Pena MA, Fierro JLG. Surface properties and catalytic performance in methane combustion of Sr-substituted lanthanum manganites. Appl Catal B 2000;24:193–205.
[14] O'Connell M, Norman AK, Haterman CF, Morris MA. Catalytic oxidation over lanthanum-transition metal perovskite materials. Catal Today 1999; 47:123–32.
[15] Buchneva G, Rosswetti I, Kryukov A. Perovskite-like catalysts for the catalytic flameless combustion of methane. Catal Industry 2012;4:121–8.
[16] Arai H, Yamada T, Eguchi K, Seiyama T. Catalytic combustion of methane over various perovskite type oxides. Appl Catal 1986;26:265–76.

[17] Seiyama T. In: Tejuka LG, Fierro GLG, editors. Preparation and application of perovskite-type oxides. Marcel Decker; 1993. p. 215.
[18] Tanaka H, Tan I, Uenishi M, Kimura M, Dohmae K. Regeneration of palladium subsequent to solid solution and segregation in a perovskite catalyst: an Intelligent catalyst. Top Catal 2001;16–17:63–70.
[19] Seyfi B, Baghalha M, Kazeman h. Modified $LaCoO_3$ nano-perovskite catalysts for the environmental application of automotive CO oxidation. Chem Eng J 2009;143:306–11.
[20] Merino NA, Barbero BP, Grange P, Cadus LE. $La_{1-x}Ca_xCoO_3$ perovskite-type oxides: preparation, characterization, stability, and catalytic potentiality for the total oxidation of propane. J Catal 2005;231:232–44.
[21] Kucharczyk B, Tylus W. Partial substitution of lanthanum with silver in the $LaMnO_3$ perovskite: effect of the modification on the activity of monolithic catalysts in the reactions of methane and carbon oxide oxidation. Appl Catal, A 2008;335:28–36.
[22] Shengelaya A, Zhao Guo-meng, Keller H, Muller KA. EPR evidence of Jahn–Teller polaron formation in $La_{1-x}Ca_xMnO_{3+y}$. Phys Rev Lett 1996;77:5296–9.
[23] Oliva C, Forni L, Pasqualin P, D'Ambrosio A, Vishniakov AV. EPR analysis of $La_{1-x}M_xMnO_{3+y}$ (M = Ce, Eu, Sr) perovskitic catalysts for methane oxidation. Phys Chem Chem Phys 1999;1:355–60.
[24] Oliva C, Forni L, D'Ambrosio A, Navarrini F, Stepanov AD, Kagramanov ZD, et al. Characterization by EPR and other techniques of $La_{1-x}Ce_xCoO_{3+delta}$ perovskite-like catalysts for methane flameless combustion. Appl Catal, A 2001;205:245–52.
[25] Nishihata Y, Mizuki J, Akao T, Tanaka H, Uenishi M, Kimura M, et al. Self-regeneration of a Pd-perovskite catalyst for automotive emissions control. Nature 2002;418:164–7.
[26] Doroftei C, Popa PD, Iacomi F. Synthesis of nanocrystalline La–Pb–Fe–O perovskite and methanol-sensing characteristics. Sens Actuators, B 2012;161:977–81.
[27] Doroftei C, Popa PD, Rezlescu N. The influence of the heat treatment on the humidity sensitivity of magnesium nanoferrite. J Optoelectron Adv Mater 2010;12(4):881–4.
[28] Popa PD, Rezlescu N, Iacob Gh. A new procedure for preparing ferrite powders. Romanian patent no. 121300, OSIM, Bucharest; 2008.
[29] Rezlescu N, Rezlescu E, Popa PD, Popovici E, Doroftei C, Ignat M. Preparation and characterization of spinel-type $MeFe_2O_4$ (Me = Cu, Cd, Ni and Zn) for catalyst applications. Mater Chem Phys 2013;137:922–7.
[30] Rezlescu N, Rezlescu E, Popa PD, Doroftei C, Ignat M. Nanostructured $GdAlO_3$ perovskite, a new possible catalyst for combustion of volatile organic compounds. J Mater Sci 2013;48:4297–304.
[31] Rezlescu N, Popa PD, Rezlescu E, Doroftei C. Microstructure characteristics of some polycrystalline oxide compounds prepared by sol–gel-selfcombustion way for gas sensor applications. Rom J Phys 2008;53(3–4):545–55.
[32] Lowell S, Shields JE, Thomas MA, Thommes M. Characterization of porous solids and powders: surface area, pore size and density. Dordrecht (Boston, London): Kluwer Academic Publishers; 2004.
[33] Pyatnitskii YuI, Bostan AI, Raevskaza LN, Nedil'ko SA, Dzyaz'ko AG, Zen'kovich EG. Theor Exp Chem 2005;41:117–21.
[34] Florea M, Alifanti M, Parvulescu VI, Mihaila-Tarabasanu D, Diamandescu L, Feder M, et al. Total oxidation of toluene on ferrite-type catalysts. Catal Today 2009;141:361–8.
[35] Milt VG, Spretz R, Ulla MA, Lombardo EA. The nature of active sites for the oxidation of methane on La-based perovskites. Catal Lett 1996;42:57–63.
[36] Song KS, Klvana D, Kirchnerova J. Kinetics of propane combustion over $La_{0.66}Sr_{0.34}Ni_{0.3}Co_{0.7}O_3$ perovskite. Appl Catal, A 2001;213:113–21.
[37] Ivanov DV, Pinaeva LG, Sadovskaya EM, Isupova LA. Influence of the mobility of oxygen on the reactivity of $La_{1-x}Sr_{(x)}MnO_3$ perovskites in methane oxidation. Kinet Catal 2011;52:401–8.
[38] Yakovleva IS, Isupova IA, Rogov VA, Sadykov VA. Forms of oxygen in $La_{1-x}Ca_xMnO_{3+delta}$ ($x = 0–1$) perovskites and their reactivities in oxidation reactions. Kinet Catal 2008;49:261–70.
[39] Isupova LA, Yakovleva IS, Alikina GM, Rogov VA, Sadykov VA. Reactivity of $La_{(1-x)}Sr_{(x)}FeO_{(3-y)}$ ($x = 0–1$) perovskites in oxidation reactions. Kinet Catal 2005;46:729–35.
[40] Marchetti L, Forni L. Catalytic combustion of methane over perovskites. Appl Catal, B 1998;15:179–87.
[41] Li WB, Wang JX, Gong H. Catalytic combustion of VOCs on non-noble metal catalysts. Catal Today 2009;148:81–7.
[42] Kundakovic L, Flytzani-Stefanopoulos M. Cu- and Ag-modified cerium oxide catalysts for methane oxidation. J Catal 1998;179:203–21.